THE JOURNAL OF PHYSICAL CHEMISTRY C

Article

Cite This: J. Phys. Chem. C 2019, 123, 28437−28442

pubs.acs.org/JPCC

Pressure-Induced Structural Phase Transformation and Yield Strength of AlN

Hong Yu,[†] Fang Peng,[*,†] Hao Liang,[†] Shixue Guan,[†] Lijie Tan,[†,‡] Zhengbi Xiong,[†] Xiaojun Xiang,[†] Qingze Li,[†] Li Lei,[†] and Duanwei He[†]

[†]Institute of Atomic and Molecular Physics, Sichuan University, Chengdu 610065, People's Republic of China

[‡]Center for High Pressure Science and Technology Advanced Research (HPSTAR), Shanghai 201203, China

Supporting Information

ABSTRACT: Aluminum nitride, a significant ceramic material used in electronic technological applications, was investigated by in situ synchrotron radiation X-ray diffraction in a diamond anvil cell at ambient temperature. The starting sample of AlN powder with a 1−2 μm average grain size was compressed to 36.9 GPa under the hydrostatic condition and 36.2 GPa under the nonhydrostatic condition, respectively. The phase transformation from hexagonal wurtzite to cubic rock salt (B4-to-B1) for the hydrostatic condition 20.5 and 20.4 GPa for the nonhydrostatic condition. We found that the phase transition was irreversible and that pure cubic phase AlN was obtained after pressure relief to reestablish ambient pressure. The experimental results reveal that the bulk modulus of hexagonal AlN is B_0 = 287.1 GPa at a fixed B_0' = 4 under hydrostatic compression. For the recompressed pure cubic sample in the diamond anvil, the equation of state (EOS) of cubic AlN is B_0 = 357.0 GPa when fit from ambient pressure to 39.5 GPa. The high pressure leads to the changes of atomic positions, bond distances, and bond angles, which were obtained from analysis using the refined GSAS package software, and explains the phase transition mechanism of hexagonal to cubic structure. In addition, the hexagonal AlN starts to exhibit a plastic deformation at approximately 8.5 GPa under nonhydrostatic compression, which is very close that of TiN by comparison.

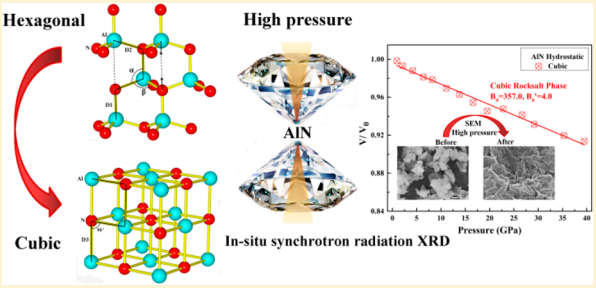

1. INTRODUCTION

The III−V nitrides have long been regarded as promising for semiconductor device applications. Aluminum nitride (AlN), an important semiconductor, is an extremely hard ceramic material in III−V nitrides with high thermal conductivity (200 W/mK), high melting point (~3070 K), and a large band gap (6.2 eV).[1,2] The discovery of stable nitrogen under high pressure makes the nitrides potential high energy density materials.[3] Due to the outstanding optical properties and unique electronic and piezoelectric properties, AlN has become an attractive high tech electronic device for use in surface acoustic wave device applications.[1,4] AlN shows excellent mechanical properties as an extraordinarily hard ceramic and remains in a stable hexagonal wurtzite (B4) structure at ambient pressure, which is similar to GaN and InN in the III−V nitrides. With regard to microsized AlN, it exhibits metal-like plastic flow under uniaxial compression at ambient temperature, as concluded by J. J. Guo et al.[5] Previous high pressure studies have proven that AlN experiences a structural change from wurtzite-type (space group $P6_3mc$) to rock-salt-type (space group $Fm3m$), which is also known as B4-to-B1 phase transformation.[4,6] Upon compression to 22.9 GPa,[7] when studied by in situ X-ray diffraction in a diamond cell (DAC), wurtzite micron AlN starts to transform to the rock salt structure phase. However, this pressure is substantially higher than the 14.5 GPa obtained from the nanosized sample by using the same method.[8] L. H. Shen et al.[9] reported that the transition of AlN nanowires is observed at the pressure of 24.9 GPa, which is much higher than that of the nanosized sample and even higher than the microsized sample, although they exhibit a similar bulk modulus and volume collapse. At the same time, several theoretical research projects were carried out and a series of conclusions were drawn on the basis of first-principle calculations.[10,11] However, the pressure-induced AlN atomic positions, bond distances, and bond angles during the structural phase transition still remain incomplete at present. Hence, it is considered essential to obtain the phase transformation mechanism of AlN to probe its potential physical and chemical properties that determine the structure−property relationships. In addition, the equation of state (EOS) of cubic AlN in previous studies was fitted from the phase transition pressure of approximately 20 GPa. In this paper, by using angle-dispersive synchrotron X-ray diffraction (ADXRD),[12,13] we complement the data before transition and obtain a relatively more precise fitted bulk modulus from ambient pressure to 39.5 GPa.

Apart from the structural phase transformation and bulk modulus, exploring the strength of AlN is also critical for high

Received: August 5, 2019
Revised: October 28, 2019
Published: October 28, 2019

DOI: 10.1021/acs.jpcc.9b07459
J. Phys. Chem. C 2019, 123, 28437−28442

technology applications. Previous studies have obtained the pressure dependence of the bulk modulus, Young's modulus, and shear modulus by using different methods,[14,15] but research on the yield strength of AlN under the nonhydrostatic condition is rarely performed by using in situ synchrotron radiation X-ray diffraction technology. Hence, it is necessary to carry out relevant research to supply the experimental data in this field. In addition, the crystal elastic modulus under high pressure has likely become accessible by means of the interpretation of X-ray diffraction line-width data for the hexagonal system derived from nonhydrostatic compression.[16,17] Therefore, the diffraction line-width data would be used for determining the compressive strength as a function of pressure. The compression properties and yield strength of AlN under nonhydrostatic compression are discussed in this paper.

2. EXPERIMENTAL PROCEDURES

High quality commercial polycrystalline AlN powder with grain size of 1−2 μm and 99.9% purity was purchased from Shanghai Xiangtian Nano Materials Co. Ltd. X-ray diffraction (XRD) was used for characterizing the crystal purity and structure (shown in Figure 1).

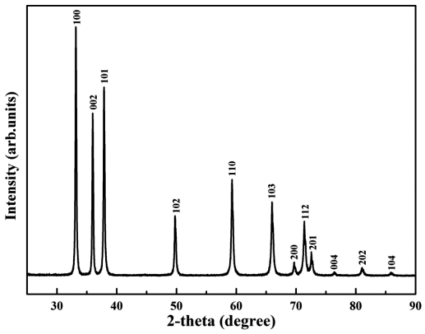

Figure 1. X-ray diffraction pattern (λ = 1.5404 Å) of initial sample at ambient conditions.

A symmetrical diamond anvil cell (DAC) with a pair of 300 μm culets was used to perform the high pressure experiments. In the first experiment, AlN polycrystals with liquid pressure transmission medium (methanol/ethanol 4:1) were loaded into a 100 μm hole of a T301 steeliness gasket that was preloaded to approximately 20 μm thickness at ~20 GPa. The liquid pressure transmitting medium (PTM) was used to maintain a hydrostatic environment for the sample under pressure. A small ruby ball of approximately ~10 μm was loaded near the central point of the sample chamber, and the ruby fluorescence shift was used for calibrating the pressure.[18] In the second experiment, all other conditions remained the same, except that there was no liquid pressure transmitting medium. In the third experiment, the pressure transmission medium was changed to silicone oil, and the other initial conditions remained the same as those of the first experiment. All three experiments were undertaken at room temperature.

The in situ high pressure synchrotron radiation angle-dispersive X-ray diffraction (ADXRD) experiments were performed in the 4W2 beamline of the Beijing Synchrotron Radiation Facility (BSRF) at ambient temperature. In all experiments, an incident synchrotron radiation X-ray beam derived from a pair of Kirkpatrick−Baez mirrors with 0.6199 Å wavelength was used to create the spot size of approximately ~20 × 30 μm^2. A CeO_2 standard was used for calibrating the geometric parameters and the distance between the sample and detector, and the average acquisition time was 100 s for each experiment at the high pressure station. The Bragg diffraction rings were recorded with a Mar-345 imaging plate detector. Fit2D software was applied to obtain the two-dimensional diffraction patterns and the 2θ intensity diffraction curves. The full width at half-maximum (fwhm) values of diffraction lines were obtained by PeakFit software. The lattice parameters and structural refinements were performed by the Rietveld method using the GSAS program as implemented in the EXPGUI package.

3. RESULTS AND DISCUSSION

3.1. Compression Behavior of AlN Powder. In Figure 2a,b, we show the variations of the X-ray diffraction patterns of

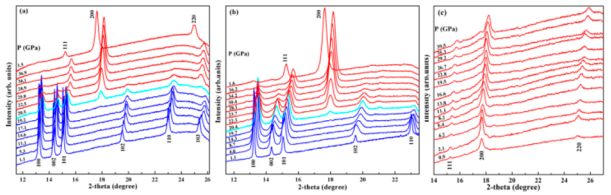

Figure 2. High pressure X-ray diffraction patterns of AlN: (a) initial hexagonal AlN under the hydrostatic condition, (b) initial hexagonal AlN under the nonhydrostatic condition, (c) initial cubic AlN under the hydrostatic condition. Note: The single cyan curve in parts a and b denotes the appearance of a new peak of the cubic rock salt phase of AlN.

the AlN up to 36.9 GPa under hydrostatic compression and 36.2 GPa under nonhydrostatic compression at room temperature, respectively. The unit cell parameters of the hexagonal AlN at ambient pressure are a = 3.1116 Å, c = 4.9801 Å, and V = 41.76 Å^3, which are in good agreement with previous ambient pressure data.[7] No changes were observed with increasing pressure up to 19.2 GPa, indicating that the samples still remained in the hexagonal phase. Upon further compression with the pressure reaching 20.5 GPa, a new peak at approximately 17.5° appeared in the X-ray diffraction patterns as shown in Figure 2a. With pressure higher than 25.8 GPa, all peaks in the hexagonal wurtzite phase are much weakened. Instead, two distinctive peaks appear and could be assigned as (111) and (200) reflections of the cubic rock-salt-type lattice. The two phases coexist in the range from 20.5 to 28.9 GPa. Upon elevation of pressure to 30.1 GPa, only the cubic rock salt phase could be identified. Compared to Figure 2a, there are some differences and similarities in Figure 2b with no pressure transmitting medium (PTM) used in the sample chamber. The two phases coexist in the range from 20.4 to 34.2 GPa, which constitues a larger pressure range. Under the nonhydrostatic condition, the new peak of the cubic rock salt phase started to emerge at the pressure of 20.4 GPa, which is almost identical to the transformation pressure of 20.5 GPa observed under the hydrostatic condition by using the same technique. The methanol−ethanol (4:1) pressure medium could maintain a hydrostatic state for pressures up to a maximum of 20 GPa; above 20 GPa, the liquid medium might undergo solidification, which leads to quasihydrostaticity in the sample chamber. The observed transformation pressure is very close to the hydrostatic pressure range, so the effect of the liquid medium is able to maintain a hydrostatic condition in

DOI: 10.1021/acs.jpcc.9b07459
J. Phys. Chem. C 2019, 123, 28437−28442

the sample chamber. Thus, it may be concluded that the transformation pressure of AlN exhibits little difference between the hydrostatic and nonhydrostatic conditions. Moreover, it is observed that all of the diffraction peaks of AlN gradually shifted to higher angles and exhibited broadened widths with increasing pressure. Upon the release of pressure to approximately 1.5 GPa and at ambient pressure, AlN still retains the diffraction peaks of the rock salt phase, which demonstrates the occurrence of the irreversible phase transformation.

To obtain a complete compression curve of pure cubic AlN from ambient to high pressure conditions, we compressed the hexagonal AlN in a DAC up to approximately 30 GPa to completely transform the samples to the cubic phase, then gradually released pressure to reach ambient pressure, and ultimately repressurized the cubic AlN sample to 39.5 GPa: the following X-ray diffraction spectra are shown in Figure 2c.

Figure 3a shows the relative volume of AlN with increasing pressure under the hydrostatic condition. A fit to the Birch–

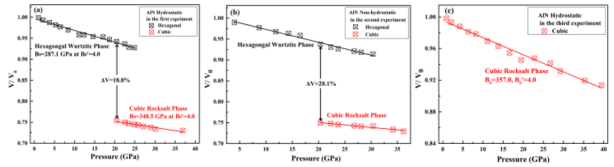

Figure 3. Equation of state (EOS) curves and the relative volumetric variations of AlN with increasing pressure under the hydrostatic condition (a), the nonhydrostatic condition (b), and initial cubic AlN under the hydrostatic condition (c), respectively. The squares indicate the hexagonal wurtzite phase AlN, and the circles indicate the cubic rock salt phase AlN.

Murnaghan equation of state (EOS) of the hexagonal wurtzite AlN phase results in the bulk modulus value B_0 = 287.1 GPa at a fixed B_0' = 4.0, which is significantly lower than the B_0 = 321 GPa value at a fixed B_0' = 4.0 for the nanosized AlN sample.[8] However, the cubic rock salt AlN gives the bulk modulus value of B_0 = 348.5 GPa at a fixed B_0' = 4.0, just slightly lower than that of nanosized AlN crystals (B_0 = 359 GPa, B_0' = 4.0).[7] Importantly, we obtained a fitted equation of state of pure cubic AlN from ambient pressure to 39.5 GPa for the repressurized sample in the DAC, and the bulk modulus value is estimated as B_0 = 357.0 GPa at a fixed B_0' = 4.0. This result is very close that of the nanosized sample obtained above the initial pressure of 14.5 GPa.[8] Previous studies indicate that the decrease of particle size results in an obvious enhancement of bulk modulus and a decline of phase transformation pressure.[7,19] However, this is only appropriate for nanocrystals with sizes of approximately 10 nm: due to size-induced volume expansion, there is no significant effect on micron samples.

The volume reduction at transformation pressure is approximately 18.8%, which is also lower than the volume reduction of 20.5% obtained from the experiment of Wang et al.[7] This is probably caused by the pressure-induced increase in the particle size.[20] Under the nonhydrostatic condition, the volume reduction at 20.4 GPa is 20.1%, as shown in Figure 3b. The detailed comparison of the high pressure parameters is listed in Table 1.

Figure 4 shows the compared SEM images of the initial AlN sample and the sample compressed to 39.5 GPa, respectively.

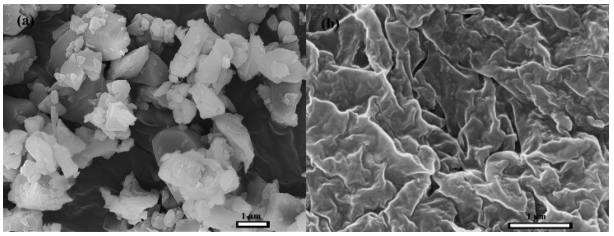

Figure 4. Scanning electron microscope (SEM) images of the initial AlN sample (a) and the sample after DAC compression (b) in the third experiment.

The crystalline morphology exhibits a significant change after a high pressure application. In Figure 4a, the starting samples manifest a clear grain shape, and it is easy to differentiate between grains. However, in Figure 4b, the shape character almost entirely disappeared after compression, and the grains huddled together; it is difficult to observe the crystal boundary under high pressure, which results from the disappearance of the hexagonal phase and the growth of a new cubic phase. Interestingly, we found that many folds appeared in the morphology, which were probably caused by the microscale

Table 1. Parameters for the Transformation from Wurtzite to Rock Salt Phase for AlN

method	particle size	transformation pressure (GPa)	pressure gauge	PTM[a]	ΔV (%)	phase	B_0 (GPa)	B_0'	ref
X-ray diffraction	5 μm	22.9	ruby	MEW[b]	18	h	207.9	6.3	8
X-ray diffraction	10 nm	14.5	Pt	ME[c]	20.5	h	321	4.0	7
						c	359	4.0	
X-ray diffraction	nano- wires	24.9	ruby	MEW	20.0	h	304	4.0	9
X-ray diffraction	1–2 μm	20.5	ruby	ME	18.8	h	287.1	4.0	this work
						c	348.5	4.0	
X-ray diffraction	1–2 μm	20.4	ruby	none	20.1				this work
X-ray diffraction	1–2 μm		ruby	silicone oil		c	357.0	4.0	this work
SHG[d]	100 nm	18	ruby	Ne					21
shock wave	4–7 μm	19.2			21	c	304	3.9	22
			Calculation						
LDA[e]		9.2			20.1		209	3.7	11
LDA		20.91			20.67		207.84	3.87	10
GGA[f]		26.91			20.43		197.83	3.84	10

[a]PTM: pressure transmitting medium. [b]MEW: methanol–ethanol–water (16:3:1). [c]ME: methanol–ethanol (4:1). [d]SHG: second harmonic generation. [e]LDA: local density approximation. [f]GGA: generalized gradient approximation.

DOI: 10.1021/acs.jpcc.9b07459
J. Phys. Chem. C 2019, 123, 28437–28442

squeezing between grains in various directions. In other words, the mutual extrusion in AlN cell structures generated microstrains under high pressure, but those strains were not coincident in all directions. In addition, it can be observed through the optical system of DAC that the sample color shifted from a grayish white to black under high pressure, and this change is consistent with the results of previous study.[9]

3.2. Pressure-Induced Structural Phase Transformation Mechanism of AlN. The selected ADXRD patterns of AlN at different pressures were refined by the Rietveld method, and three of these typical spectra are shown in Figure 5. In

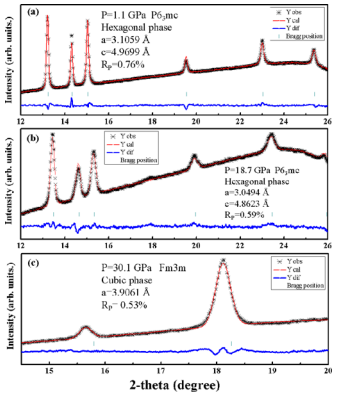

Figure 5. Three typical Rietveld refinements by the GSAS package of AlN under hydrostatic compression: (a) at a pressure of 1.1 GPa (R_{wp} = 1.06%, R_p = 0.76%, χ^2 = 3.64), (b) at a pressure of 18.7 GPa (R_{wp} = 0.80%, R_p = 0.59%, χ^2 = 2.051), and (c) at a pressure of 30.1 GPa (R_{wp} = 0.69%, R_p = 0.53%, χ^2 = 1.555), respectively. The black asterisks denote experimental data points, and red lines denote the data refinements. Blue lines denote the difference between observed values and calculated patterns, and the short green vertical lines denote the peaks of corresponding samples.

Figure 5a,b, AlN remained in the hexagonal phase with six main peaks observed. The cell parameters of the hexagonal phase AlN, a = 3.1059 Å and c = 4.9699 Å, decreased to a = 3.0494 Å and c = 4.8623 Å with a pressure increase from 1.1 to 18.7 GPa. Figure 5c shows that the phase transformation was completely finished, with only two peaks observed by experiment. After the phase transition, the cell parameter of cubic AlN changed to a = 3.9061 Å at a pressure of 30.1 GPa. Several Rietveld refinement details of AlN at various pressures are given in Table 2.

Figure 6a shows the changes in atomic bond distance and the variations of atomic structure of AlN under hydrostatic compression. Before the transformation, there are two separate Al−N distances per every unit cell, denoted D1 and D2, and two different N−Al−N angles denoted as α and β, respectively. At first, two Al−N distances are decreased gradually along with

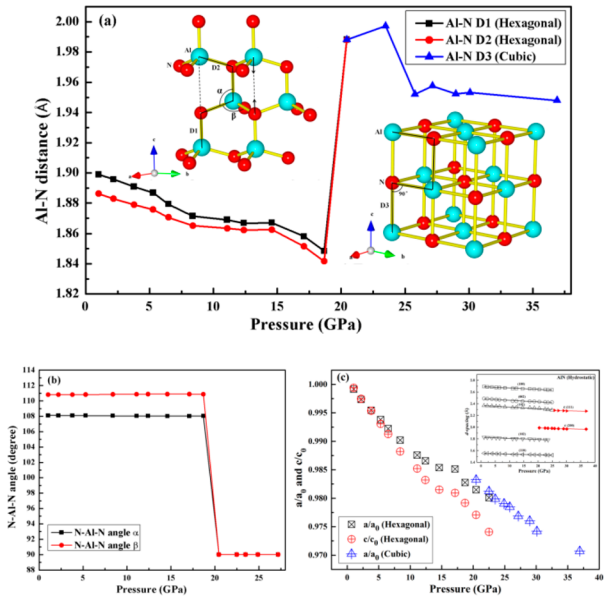

Figure 6. Pressure-induced changes in atomic (a) bond distances, (b) bond angles, and (c) cell parameter ratios (a/a_0 and c/c_0) for AlN under the hydrostatic condition. Insert for part a: AlN atomic structures of hexagonal phase and cubic phase, respectively. α and β correspond to the N−Al−N angle in part b. Insert for part c: changes of d spacing with increasing pressure for AlN under the hydrostatic condition. The hollow shapes indicate that the different reflections of the hexagonal wurtzite phase and solid shapes are for the cubic rock salt phase.

the two different N−Al−N angles with increasing pressure (Figure 6b). The cell parameters (a and c) and d spacing are slightly decreased with Al−N distances in Figure 6c. Because cell parameter c decreased faster than cell parameter a, the atoms of Al and N undergo a larger deformation in axis c. This deformation accumulates under compression, resulting in the generation of new Al−N bonds in axis c, as shown by the dotted lines in the inset of Figure 6a, and, at the same time, is accompanied by some degree of distortion between N−Al−N angles. Finally, these facts make the wurtzite hexagonal structure transform to the rock salt cubic structure. When transformation occurred, the huge increases in two different distances and enormous decreases in two distinct angles took place together. After the hexagonal wurtzite phase, AlN almost totally transformed to the cubic rock salt phase; the two different Al−N distances (D1 and D2) became one (D3) and tended to slightly decrease with the increasing pressure. Moreover, the two different angles (α and β) became a fixed value (90°) and remain unchanged with cubic structure. Table 3 shows the details of bond angles and bond distances of AlN at three different typical pressures.

Table 2. Rietveld Refinement Details of AlN at Various Pressures

crystal system		hexagonal	hexagonal	hexagonal	hexagonal	cubic	cubic	cubic
space group		$P6_3mc$	$P6_3mc$	$P6_3mc$	$P6_3mc$	$Fm3m$	$Fm3m$	$Fm3m$
pressure (GPa)		1.1	8.4	18.7	20.5	23.5	30.1	36.9
lattice constant (Å)	a	3.1059(4)	3.0809(7)	3.0494(14)	3.0332(3)	3.9943(2)	3.9061(61)	3.8958(52)
	c	4.9699(6)	4.9185(11)	4.8623(21)	4.8374(5)	3.9943(2)	3.9061(61)	3.8958(52)
cell volume (Å^3)	V	41.52(1)	40.43(2)	39.16(4)	38.54(11)	63.73(1)	59.59(28)	59.13(24)
R_p (%)		0.76	0.89	0.59	0.45	0.49	0.53	0.47
R_{wp} (%)		1.06	1.38	0.80	0.57	0.61	0.69	0.59

DOI: 10.1021/acs.jpcc.9b07459
J. Phys. Chem. C 2019, 123, 28437−28442

Table 3. Bond Angles and Bond Distances of AlN at Various Pressures

pressure (GPa)	1.1	18.7	20.5	23.5	30.1
Al−N−Al α (deg)	108.097(3)	108.038(11)	90.0	90.0	90.0
Al−N−Al β (deg)	110.804(3)	110.86(10)	90.0	90.0	90.0
Al−N D1 (Å)	1.89901(25)	1.8484(8)			
Al−N D2 (Å)	1.88633(23)	1.8416(8)			
Al−N D3 (Å)			1.9881(33)	1.9971(11)	1.9531(31)

Figure 6c shows the variations of cell parameter ratios (a/a_0 and c/c_0) for AlN under the hydrostatic condition. From the variation tendencies of a/a_0 and c/c_0, it can be observed that a/a_0 and c/c_0 maintain good isotropy for pressure up to approximately 11.1 GPa, with AlN remaining in the hexagonal structure. For pressures above 11.1 GPa, a/a_0 and c/c_0 start to show the anisotropy phenomenon. The variation tendency of a/a_0 is evidently slower than that of c/c_0, and it is reasonably suggested that cell parameter a and cell parameter c indicate different deformations under high pressure. Therefore, the phase transformation from wurtzite to rock salt occurs when sufficient deformations accumulate to exceed the limit of hexagonal structure. The inset shows the variations of d spacing with increasing pressure under the hydrostatic condition. Between 20.5 and 25.8 GPa, a discontinuity appears in the d spacing of the cubic (111) reflection, which is extremely close to that of the hexagonal wurtzite (101) reflection. Therefore, the cubic (111) reflection is disturbed and could not be observed by measurement.

3.3. Yield Strength of AlN under High Pressure. The synchrotron radiation X-ray diffraction line profiles from the polycrystalline sample under nonhydrostatic uniaxial compression in a DAC exhibit broadening with the increasing pressure.[23,24] Figure 7a shows the full width at half-maximum

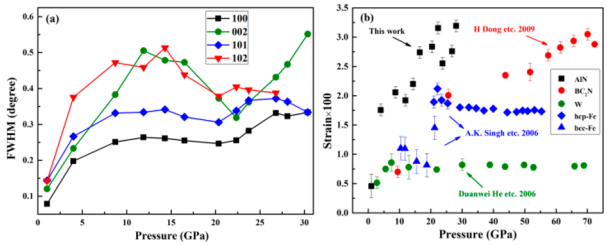

Figure 7. (a) Full width at half-maximum (fwhm) of synchrotron radiation X-ray diffraction lines with increasing pressure. (b) Deviatoric stress comparison as a function of pressure. Black squares, AlN; red circles, BC_2N;[26] green circles, W;[27] blue triangles, bcc-Fe; blue rhombi, hcp-Fe.[17]

(fwhm) values of X-ray diffraction lines of AlN under nonhydrostatic compression. Four different lines denote four different reflections. Supposing a minimal influence of grain refinement and removing the effect of instrumental parameters, the line widths become considerably wider with increasing pressure, indicating that the AlN sample undergoes elastic deformation according to the line-widths analysis theory and then exhibits the tendency to flatten with further compression until the pressure exceeds 8.5 GPa. The results imply that the AlN starts to exhibits plastic deformation under high pressure. The yield strength of AlN is similar to that of TiN, which reaches 8.6 GPa under uniaxial nonhydrostatic compression.[25] However, the flat state ended with the pressure of ∼20 GPa, and the line width appeared to display a second increase. When the pressure reached approximately 25 GPa, the line widths again flattened and then appeared to slightly decrease. The variation trends of green solid circles, which denote the hexagonal wurtzite (002) reflection, are not consistent with the other three lines: Part of the reason for this is probably that the peak shape experiences distortion under nonhydrostatic compression and leads to the fitting deviation. Owing to the nonuniform strains produced by mutual particle extrusion, the diffraction peaks appear to exhibit asymmetric deformation and result in inevitable deviations in the procession of analysis.[28] These changes may be caused by the pressure gradients of the sample chamber under the nonhydrostatic condition.

Figure 7b shows the deviatoric stresses of AlN and several other materials as functions of pressure. AlN powder samples exhibited low deviatoric stress values before uniaxial compression, which drastically increased after initial compression, and then ascended moderately with the increasing pressure and reached the highest stress values at the pressure of 28.1 GPa. In a comparison with metals such as Fe and W, AlN ceramic demonstrates higher strain with increasing pressure. This is probably because the strength of the metal is comparatively low, and the infiltration of nonmetallic elements (B, C, N) potentially enhanced the strength of materials. BC_2N has a similar strain value to that of AlN, but the strength is higher than AlN.

4. CONCLUSIONS

In conclusion, we have investigated the pressure-induced phase transformation of AlN under hydrostatic conditions and nonhydrostatic conditions by compressing the samples with pressures up to 36.9 and 36.2 GPa in DAC using in situ synchrotron radiation ADXRD at ambient temperature. The AlN sample, with an average grain size of 1−2 μm, exhibited structural phase transformation at the pressure of 20.5 GPa under the hydrostatic condition and 20.4 GPa under the nonhydrostatic condition, respectively. The mechanisms of phase transformation have been discussed in this paper, and the changes of bond distances and bond angles have been obtained from the refined GSAS package, indicating that two different bond distances (D1 and D2) drastically increased at the transformation pressure while two different bond angles (α and β) appeared to sharply decrease. The mechanism explained the production of new Al−N bonds in the AlN polycrystalline structure to make the hexagonal phase finally transform to the cubic phase. Moreover, the phase transition is irreversible, and the pure cubic AlN sample is obtained after pressure relief to re-establish ambient pressure. The bulk modulus value of pure cubic AlN is B_0 = 357.0 GPa after recompression of the sample from ambient pressure to 39.5 GPa under the hydrostatic condition. Thus, we obtain a complete compression curve of cubic AlN under high pressure. The strength and plastic deformation of AlN have been derived by analyzing X-ray diffraction peak broadening. The results reveal that the AlN sample starts to yield at approximately 8.5 GPa under nonhydrostatic compression, which yields a

DOI: 10.1021/acs.jpcc.9b07459
J. Phys. Chem. C 2019, 123, 28437−28442

strength close to that of TiN (8.6 GPa), but the deviatoric stress of AlN is higher than that of TiN.

■ ASSOCIATED CONTENT

Supporting Information

The Supporting Information is available free of charge on the ACS Publications website at DOI: 10.1021/acs.jpcc.9b07459.

Theory of synchrotron radiation X-ray diffraction line-width analysis (PDF)

■ AUTHOR INFORMATION

Corresponding Author

*E-mail: fangpeng18@yahoo.com.

ORCID

Hong Yu: 0000-0003-0299-5964

Hao Liang: 0000-0002-4965-4705

Lijie Tan: 0000-0001-9396-7613

Notes

The authors declare no competing financial interest.

■ ACKNOWLEDGMENTS

This work was supported by the joint fund of the National Natural Science Foundation of China and Scientific Instrumentation Fund of Chinese Academy of Sciences (Grant U1332104). High pressure synchrotron radiation XRD experiments were carried out in the 4W2 beamline of the Beijing Synchrotron Radiation Facility (BSRF).

■ REFERENCES

(1) Dettmer, E. S.; Romenesko, B. M.; Charles, H. K.; Carkhuff, B. G.; Merrill, D. J. In Steady state thermal conductivity measurements of AlN and SiC substrate materials. *IEEE Trans. Compon., Hybrids, Manuf. Technol.* **1989**, *12*, 543−547.

(2) Slack, G. A.; McNelly, T. F. Growth of high purity AlN crystals. *J. Cryst. Growth* **1976**, *34*, 263−279.

(3) Wang, X.; Wang, Y.; Miao, M.; Zhong, X.; Lv, J.; Cui, T.; Li, J.; Chen, L.; Pickard, C. J.; Ma, Y. Cagelike diamondoid nitrogen at high pressures. *Phys. Rev. Lett.* **2012**, *109*, 175502.

(4) Strite, S. T.; Morkoc, H. GaN, AlN, and InN: A Review. *J. Vac. Sci. Technol., B: Microelectron. Process. Phenom.* **1992**, *10*, 1237−1266.

(5) Guo, J. J.; Madhav Reddy, K.; Hirata, A.; Fujita, T.; Gazonas, G. A.; McCauley, J. W.; Chen, M. W. Sample size induced brittle-to-ductile transition of single-crystal aluminum nitride. *Acta Mater.* **2015**, *88*, 252−259.

(6) Vollstadt, H.; Ito, E.; Akaishi, M.; Akimoto, S. I.; Fukunaga, O. High pressure synthesis of rocksalt type of AlN. *Proc. Jpn. Acad., Ser. B* **1990**, *66*, 7−9.

(7) Wang, Z.; Tait, K.; Zhao, Y.; Schiferl, D.; Zha, C.; Uchida, H.; Downs, R. T. Size-induced reduction of transition pressure and enhancement of bulk modulus of AlN nanocrystals. *J. Phys. Chem. B* **2004**, *108*, 11506−11508.

(8) Ueno, M.; Onodera, A.; Shimomura, O.; Takemura, A. X-ray observation of the structural phase transition of aluminum nitride under high pressure. *Phys. Rev. B: Condens. Matter Mater. Phys.* **1992**, *45*, 10123−10126.

(9) Shen, L. H.; Li, X. F.; Ma, Y. M.; Yang, K. F.; Lei, W. W.; Cui, Q. L.; Zou, G. T. Pressure-induced structural transition in AlN nanowires. *Appl. Phys. Lett.* **2006**, *89*, 141903.

(10) Saib, S.; Bouarissa, N. Structural properties of AlN from first principles calculations. *Eur. Phys. J. B* **2005**, *47*, 379−383.

(11) Serrano, J.; Rubio, A.; Hernández, E.; Muñoz, A.; Mujica, A. Theoretical study of the relative stability of structural phases in group-III nitrides at high pressures. *Phys. Rev. B: Condens. Matter Mater. Phys.* **2000**, *62*, 16612−16623.

(12) Huang, Y.; He, Y.; Sheng, H.; Lu, X.; Dong, H.; Samanta, S.; Liu, Y.; et al. Li-ion battery material under high pressure: amorphization and enhanced conductivity of $Li_4Ti_5O_{12}$. *Natl. Sci. Rev.* **2019**, *6*, 239−246.

(13) Mao, H. K.; Chen, X. J.; Ding, Y.; Li, B.; Wang, L. Solids, liquids, and gases under high pressure. *Rev. Mod. Phys.* **2018**, *90*, 015007.

(14) Collaboration: Authors and editors of the volumes III/17A-22A-41A1a. Aluminum nitride (AlN) bulk modulus, Young's and shear modulus. *Group IV Elements, IV-IV and III-V Compounds. Part a-Lattice Properties* **2001**, 1−6.

(15) Zagorac, D.; Zagorac, J.; Djukic, M.; Jordanov, D.; Matović, B. Theoretical study of AlN mechanical behaviour under high pressure regime. *Theor. Appl. Fract. Mech.* **2019**, *103*, 102289.

(16) Singh, A. K.; Balasingh, C. The lattice strains in a specimen (hexagonal system) compressed nonhydrostatically in an opposed anvil high pressure setup. *J. Appl. Phys.* **1994**, *75*, 4956−4962.

(17) Singh, A.; Jain, A.; Liermann, H.; Saxena, S. Strength of iron under pressure up to 55 GPa from X-ray diffraction line-width analysis. *J. Phys. Chem. Solids* **2006**, *67*, 2197−2202.

(18) Mao, H. K.; Xu, J.; Bell, P. M. Calibration of the ruby pressure gauge to 800 kbar under quasi-hydrostatic conditions. *J. Geophys. Res.* **1986**, *91*, 4673−4676.

(19) Wang, Z.; Zhao, Y.; Schiferl, D.; Qian, J.; Downs, R. T.; Mao, H. K.; Sekine, T. Threshold pressure for disappearance of size-induced effect in spinel-structure Ge_3N_4 nanocrystals. *J. Phys. Chem. B* **2003**, *107*, 14151−14153.

(20) Wang, Z.; Zhao, Y.; Schiferl, D.; Zha, C. S.; Downs, R. T. Pressure induced increase of particle size and resulting weakening of elastic stiffness of CeO_2 nanocrystals. *Appl. Phys. Lett.* **2004**, *85*, 124−126.

(21) Bayarjargal, L.; Wiehl, L.; Winkler, B. r. Influence of grain size, surface energy, and deviatoric stress on the pressure-induced phase transition of ZnO and AlN. *High Pressure Res.* **2013**, *33*, 642−651.

(22) Mashimo, T.; Uchino, M.; Nakamura, A.; Kobayashi, T.; Takasawa, E.; Sekine, T.; Noguchi, Y.; Hikosaka, H.; Fukuoka, K.; Syono, Y. Yield properties, phase transition, and equation of state of aluminum nitride (AlN) under shock compression up to 150 GPa. *J. Appl. Phys.* **1999**, *86*, 6710−6716.

(23) Singh, A. K.; Liermann, H. P.; Saxena, S. K. Strength of magnesium oxide under high pressure: evidence for the grain-size dependence. *Solid State Commun.* **2004**, *132*, 795−798.

(24) Chen, J.; Weidner, D. J.; Vaughan, M. T. The strength of $Mg_{0.9}Fe_{0.1}SiO_3$ perovskite at high pressure and temperature. *Nature* **2002**, *419*, 824−6.

(25) Chen, H.; Peng, F.; Mao, H. K.; Shen, G.; Liermann, H. P.; Li, Z.; Shu, J. Strength and elastic moduli of TiN from radial X-ray diffraction under nonhydrostatic compression up to 45 GPa. *J. Appl. Phys.* **2010**, *107*, 113503.

(26) Dong, H.; He, D.; Duffy, T. S.; Zhao, Y. J. Elastic moduli and strength of nanocrystalline cubic BC_2N from X-ray diffraction under nonhydrostatic compression. *Phys. Rev. B: Condens. Matter Mater. Phys.* **2009**, *79*, 014105.

(27) He, D.; Duffy, T. S. X-ray diffraction study of the static strength of tungsten to 69 GPa. *Phys. Rev. B: Condens. Matter Mater. Phys.* **2006**, *73*, 4106.

(28) Leineweber, A.; Dinnebier, R. E. Anisotropic microstrain broadening of minium, Pb_3O_4, in a high-pressure cell: interpretation of line-width parameters in terms of stress variations. *J. Appl. Crystallogr.* **2010**, *43*, 17−26.